Real-Time Characterization of Aerospace Structures Using Onboard Strain Measurement Technologies and Inverse Finite Element Method

A. TESSLER, J. L. SPANGLER, M. MATTONE, M. GHERLONE and M. DI SCIUVA

ABSTRACT

The inverse problem of real-time reconstruction of full-field structural displacements, strains, and stresses is addressed using an inverse finite element method based on shear deformable shell finite element technology. Utilizing surface strain measurements from strain sensors mounted on load-carrying structural components, the methodology enables accurate computations of the three-dimensional displacement field for a general built-up shell structure undergoing multi-axial deformations. The strain and stress computations are then carried out at the element level using strain-displacement and constitutive relations. This high fidelity computational technology is essential for providing feedback to the actuation and control systems of the next generation of aerospace vehicles, and for assessing real-time internal loads and structural integrity.

INTRODUCTION

Structural health management systems, which by way of real-time monitoring help mitigate accidents due to structural failures, will become integral technologies of the next-generation aerospace vehicles. Advanced sensor arrays and signal processing technologies are utilized to provide optimally distributed in-situ sensor information related to the states of strain, temperature, and aerodynamic pressure. To process the massive quantities of measured data and to infer physically admissible structural behavior requires robust and computationally efficient physics-based algorithms.

The inverse Finite Element Method (*iFEM*) introduced by Tessler and co-workers [1-7] is a computational methodology that integrates sensor strain data across the entire structural domain and produces a continuous displacement field of the discretized structure, i.e., the algorithm solves an inverse problem. The method's mathematical foundation is a weighted least-squares variational principle which relies

Alexander Tessler: NASA Langley Research Center, Structural Mechanics and Concepts Branch, Mail Stop 190, Hampton, VA 23681-2199, U.S.A.
Jan L. Spangler: Lockheed Martin Aeronautics Company, Mail Stop 190, Hampton, Virginia, 23681-2199, U.S.A.
Marco Gherlone, Massimiliano Mattone, Marco Di Sciuva: Politecnico di Torino, Department of Aeronautics and Space Engineering, Corso Duca degli Abruzzi 24, 10129 Torino, ITALY.

Report Documentation Page

Form Approved
OMB No. 0704-0188

1. REPORT DATE	2. REPORT TYPE	3. DATES COVERED
SEP 2011	**N/A**	**-**

4. TITLE AND SUBTITLE
Real-Time Characterization of Aerospace Structures Using Onboard Strain Measurement Technologies and Inverse Finite Element Method

5a. CONTRACT NUMBER
5b. GRANT NUMBER
5c. PROGRAM ELEMENT NUMBER

6. AUTHOR(S)

5d. PROJECT NUMBER
5e. TASK NUMBER
5f. WORK UNIT NUMBER

7. PERFORMING ORGANIZATION NAME(S) AND ADDRESS(ES)
NASA Langley Research Center, Structural Mechanics and Concepts Branch, Mail Stop 190, Hampton, VA 23681-2199, U.S.A.

8. PERFORMING ORGANIZATION REPORT NUMBER

9. SPONSORING/MONITORING AGENCY NAME(S) AND ADDRESS(ES)

10. SPONSOR/MONITOR'S ACRONYM(S)
11. SPONSOR/MONITOR'S REPORT NUMBER(S)

12. DISTRIBUTION/AVAILABILITY STATEMENT
Approved for public release, distribution unlimited

13. SUPPLEMENTARY NOTES
See also ADA580921. International Workshop on Structural Health Monitoring: From Condition-based Maintenance to Autonomous Structures. Held in Stanford, California on September 13-15, 2011 . U.S. Government or Federal Purpose Rights License.

14. ABSTRACT
The inverse problem of real-time reconstruction of full-field structural displacements, strains, and stresses is addressed using an inverse finite element method based on shear deformable shell finite element technology. Utilizing surface strain measurements from strain sensors mounted on load-carrying structural components, the methodology enables accurate computations of the three-dimensional displacement field for a general built-up shell structure undergoing multi-axial deformations. The strain and stress computations are then carried out at the element level using strain-displacement and constitutive relations. This high fidelity computational technology is essential for providing feedback to the actuation and control systems of the next generation of aerospace vehicles, and for assessing realtime internal loads and structural integrity.

15. SUBJECT TERMS

16. SECURITY CLASSIFICATION OF:			17. LIMITATION OF ABSTRACT	18. NUMBER OF PAGES	19a. NAME OF RESPONSIBLE PERSON
a. REPORT	b. ABSTRACT	c. THIS PAGE			
unclassified	**unclassified**	**unclassified**	**SAR**	**8**	

on the discretization of structural geometry by any type of structural element including beam, frame, plate, shell, and solid. Displacement boundary conditions and in situ strain measurements are used as prescribed input quantities imposed on a model. The discretized model results in a system of linear algebraic equations that has a nonsingular square matrix dependent on the strain-sensor positions. For a given model and fixed strain-sensor locations, the matrix is decomposed (inverted) only once. The right-hand-side vector is a function of the strain values that change as the structure deforms under loading. Thus, the computational algorithm involves multiplication of a matrix, that stays unchanged, and a right-hand-side vector that is recomputed in real time, reflecting changes in strain-sensor readings during deformation. The algorithm is capable of producing reliable and accurate displacement predictions of structural deformations in real time. The reconstructed displacements are then used to compute strains, stresses, and failure criteria, thus providing the requisite information for an onboard structural-integrity analysis tool.

This paper discusses the latest advances in the *iFEM* formulation for built-up plate and shell structures aimed at constructing the full-field displacements, strains, and stresses from strain data provided by in-situ strain sensors. The application focus is on the stain data obtained from FBG (Fiber Bragg Grating) sensor arrays that provide either single-core (axial) or rosette (tri-axial) strain measurements. The new formulation is based upon the minimization of a weighted-least-squares functional that uses the complete set of strain measures corresponding to the first-order shear deformation theory. The error functional uses the least-squares-difference terms comprised of the strain measures which are expressed in terms of the assumed element displacements and the corresponding strains that are measured experimentally. All strain-displacement relations are enforced explicitly whereas the analytical and measured strains are matched in the least-squares sense. By virtue of these assumptions, all strain compatibility relations are explicitly satisfied. The methodology does not require elastic or inertial material properties. The inverse shell element used is a three-node triangle which has six conventional degrees-of-freedom at each node, i.e., three displacements and three rotations. The kinematic variables are interpolated using the lowest-order anisoparametric C^0-continuous functions, i.e., linear in-plane displacements and bending rotations, and a constrained-type quadratic deflection. These functions were adopted from an earlier plate-element formulation [8]. The formulation is implemented as a user-element routine in the ABAQUS code [9]; the latter is used as an engine for solving the algebraic equations resulting from *iFEM* models, as well as a pre- and post-processing tool.

A computational example is presented for a statically loaded cantilevered plate for which experimentally measured strains are represented (or simulated) by strain results obtained by a high-fidelity solution using the ABAQUS finite element code. The input surface strains are only provided along sparsely distributed lines to simulate strain data from FBG (Fiber Bragg Grating) arrays that provide either single-core (axial) or rosette (tri-axial) strain measurements. Several types of discretization strategies are examined and comparisons of the reconstructed *iFEM* and direct *FEM* displacement solutions are provided. It is demonstrated that in the absence of available sensor-strain data and under conditions of relatively sparse sensor-strain data, it is possible to reconstruct a relatively accurate deformed structural shape even on high-fidelity meshes by exploiting judiciously the weighting function capability of the methodology.

FORMULATION OF INVERSE SHELL ELEMENT

Using Mindlin-theory kinematic assumptions, the three components of the displacement vector $\mathbf{u} = (u_x, u_y, u_z)$ in the local Cartesian reference frame of a three-node inverse shell element, *iMIN3*, are defined as (refer to Figure 1):

$$u_x(x,y,z) = u + z\,\theta_y, \quad u_y(x,y,z) = v + z\,\theta_x, \quad u_z(x,y,z) = w \tag{1}$$

where $u = u(x,y)$ and $v = v(x,y)$ are the mid-plane displacements in the x and y directions, respectively; $\theta_x = \theta_x(x,y)$ and $\theta_y = \theta_y(x,y)$ are the rotations of the normal about the negative x and positive y axes, respectively; and $w = w(x,y)$ is the deflection variable which is constant across the thickness coordinate $z \in [-t,t]$, with $2t$ denoting the total shell thickness.

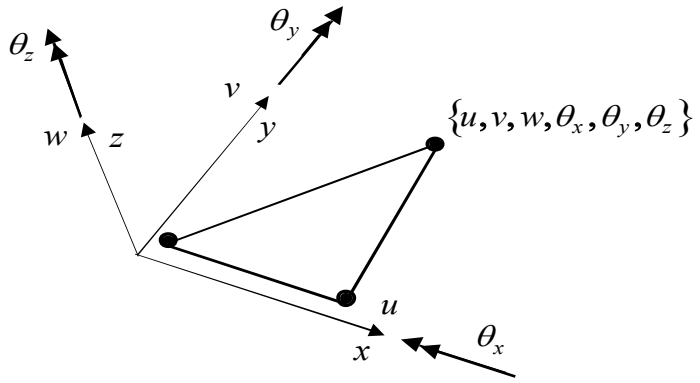

Figure 1. *iMIN3*: a three-node inverse shell element.

The strain-displacement relations, taking into account Eqs. (1), have the form

$$\begin{Bmatrix} \varepsilon_{xx} \\ \varepsilon_{yy} \\ \gamma_{xy} \end{Bmatrix} = \begin{Bmatrix} \varepsilon_{x0} \\ \varepsilon_{y0} \\ \gamma_{xy0} \end{Bmatrix} + z \begin{Bmatrix} \kappa_{x0} \\ \kappa_{y0} \\ \kappa_{xy0} \end{Bmatrix} \equiv \mathbf{e}(\mathbf{u}) + z\,\mathbf{k}(\mathbf{u}) \tag{2}$$

where the membrane strain measures associated with the stretching of the middle surface are given as

$$\mathbf{e}(\mathbf{u}) \equiv \begin{Bmatrix} \varepsilon_{x0} \\ \varepsilon_{y0} \\ \gamma_{xy0} \end{Bmatrix} = \begin{bmatrix} \frac{\partial}{\partial x} & 0 & 0 & 0 & 0 \\ 0 & \frac{\partial}{\partial y} & 0 & 0 & 0 \\ \frac{\partial}{\partial y} & \frac{\partial}{\partial x} & 0 & 0 & 0 \end{bmatrix} \begin{Bmatrix} u \\ v \\ w \\ \theta_x \\ \theta_y \end{Bmatrix} \equiv \mathbf{L}^m\,\mathbf{u} \tag{3}$$

and the bending curvatures are

$$\mathbf{k}(\mathbf{u}) \equiv \begin{Bmatrix} \kappa_{x0} \\ \kappa_{y0} \\ \kappa_{xy0} \end{Bmatrix} = \begin{bmatrix} 0 & 0 & 0 & 0 & \frac{\partial}{\partial x} \\ 0 & 0 & 0 & \frac{\partial}{\partial y} & 0 \\ 0 & 0 & 0 & \frac{\partial}{\partial x} & \frac{\partial}{\partial y} \end{bmatrix} \begin{Bmatrix} u \\ v \\ w \\ \theta_x \\ \theta_y \end{Bmatrix} \equiv \mathbf{L}^b \mathbf{u} \tag{4}$$

The transverse shear strains can also be expressed in terms of the same five kinematic variables as

$$\mathbf{g}(\mathbf{u}) \equiv \begin{Bmatrix} \gamma_{xz0} \\ \gamma_{yz0} \end{Bmatrix} = \begin{bmatrix} 0 & 0 & \frac{\partial}{\partial x} & 0 & 1 \\ 0 & 0 & \frac{\partial}{\partial y} & 1 & 0 \end{bmatrix} \begin{Bmatrix} u \\ v \\ w \\ \theta_x \\ \theta_y \end{Bmatrix} \equiv \mathbf{L}^s \mathbf{u} \tag{5}$$

Assuming the structure is instrumented with strain sensors (e.g., conventional strain rosettes or fiber-optic Bragg-grating sensors), strains are measured at the locations $\mathbf{x}_i = (x_i, y_i, \pm t)$ representing the top and bottom shell surfaces. Evaluating Eqs. (2) at these discrete locations, the relationships between the measured surface strains and the reference plane strains and curvatures can be readily established as

$$\mathbf{e}_i^{\varepsilon} \equiv \begin{Bmatrix} \varepsilon_{x0}^{\varepsilon} \\ \varepsilon_{y0}^{\varepsilon} \\ \gamma_{xy0}^{\varepsilon} \end{Bmatrix}_i = \frac{1}{2}\left(\begin{Bmatrix} \varepsilon_{xx}^{+} \\ \varepsilon_{yy}^{+} \\ \gamma_{xy}^{+} \end{Bmatrix}_i + \begin{Bmatrix} \varepsilon_{xx}^{-} \\ \varepsilon_{yy}^{-} \\ \gamma_{xy}^{-} \end{Bmatrix}_i \right), \quad \mathbf{k}_i^{\varepsilon} \equiv \begin{Bmatrix} \kappa_{x0}^{\varepsilon} \\ \kappa_{y0}^{\varepsilon} \\ \kappa_{xy0}^{\varepsilon} \end{Bmatrix}_i = \frac{1}{2t}\left(\begin{Bmatrix} \varepsilon_{xx}^{+} \\ \varepsilon_{yy}^{+} \\ \gamma_{xy}^{+} \end{Bmatrix}_i - \begin{Bmatrix} \varepsilon_{xx}^{-} \\ \varepsilon_{yy}^{-} \\ \gamma_{xy}^{-} \end{Bmatrix}_i \right) \tag{6, 7}$$

where ε signifies the existence of experimental error in the strain measurements and, hence, in $\mathbf{e}_i^{\varepsilon}$ and $\mathbf{k}_i^{\varepsilon}$.

VARIATIONAL FRAMEWORK AND THREE-NODE INVERSE SHELL ELEMENT

Using the aforementioned kinematic assumptions, a simple and versatile *inverse shell element* is developed consisting of three nodes and six engineering degrees-of-freedom (dof's) at each node, as illustrated in Figure 1. To avoid singular solutions in the modeling of built-up shell structures, a drilling rotation, θ_z, degree-of-freedom can be readily added.

The element matrices are derived using a weighted-least-squares smoothing functional, for which a stationary value is sought by minimization with respect to the unknown displacement degrees-of-freedom. For an inverse shell finite element of area A_e, this functional can be expressed as

$$\Phi_e(\mathbf{u}) = w_e \left\| \mathbf{e}(\mathbf{u}) - \mathbf{e}^{\varepsilon} \right\|^2 + w_k \left\| \mathbf{k}(\mathbf{u}) - \mathbf{k}^{\varepsilon} \right\|^2 + w_g \left\| \mathbf{g}(\mathbf{u}) - \mathbf{g}^{\varepsilon} \right\|^2 \tag{8}$$

where the squared norms are given as

$$\begin{aligned}
\left\| \mathbf{e}(\mathbf{u}) - \mathbf{e}^{\varepsilon} \right\|^2 &\equiv \frac{1}{n} \int_{A_e} \sum_{i=1}^{n} \left[\mathbf{e}(\mathbf{u})_i - \mathbf{e}_i^{\varepsilon} \right]^2 d\mathrm{x}\, d\mathrm{y}, \\
\left\| \mathbf{k}(\mathbf{u}) - \mathbf{k}^{\varepsilon} \right\|^2 &\equiv \frac{(2t)^2}{n} \int_{A_e} \sum_{i=1}^{n} \left[\mathbf{k}(\mathbf{u})_i - \mathbf{k}_i^{\varepsilon} \right]^2 d\mathrm{x}\, d\mathrm{y}, \\
\left\| \mathbf{g}(\mathbf{u}) - \mathbf{g}^{\varepsilon} \right\|^2 &\equiv \frac{1}{n} \int_{A_e} \sum_{i=1}^{n} \left[\mathbf{g}(\mathbf{u})_i - \mathbf{g}_i^{\varepsilon} \right]^2 d\mathrm{x}\, d\mathrm{y}
\end{aligned} \tag{9.1}$$

in which $n \geq 1$ is the number of strain sensor locations that fall within the element domain, and $\left(w_e, w_k, w_g \right)$ are the weighting coefficients. The procedure, leading up to Eqs. (6) and (7), gives rise to $\mathbf{e}_i^{\varepsilon}$ and $\mathbf{k}_i^{\varepsilon}$ that are computed from the in-situ strains that are measured by strain sensors; however, the experimental transverse shear measures, $\mathbf{g}_i^{\varepsilon}$, cannot be directly obtained from the surface strains. To determine $\mathbf{g}_i^{\varepsilon}$, the analytic plate equilibrium equations that relate the transverse-shear forces to the bending moments can be used [4].

The key advantage of this revised variational formulation rests on the introduction of the weighting coefficients $\left(w_e, w_k, w_g \right)$ in Eq. (8). This seemingly small change in the element functional $\Phi_e(\mathbf{u})$, compared to the original form, permits the use of high-fidelity discretizations even when the measured strain data are sparse, as it is often the case when FBG sensors are used. For an inverse element without strain-sensor data, the squared norms are given as

$$\begin{aligned}
\left\| \mathbf{e}(\mathbf{u}) - \mathbf{e}^{\varepsilon} \right\|^2 &\equiv \int_{A_e} \mathbf{e}(\mathbf{u})^2 d\mathrm{x}\, d\mathrm{y}, \\
\left\| \mathbf{k}(\mathbf{u}) - \mathbf{k}^{\varepsilon} \right\|^2 &\equiv (2t)^2 \int_{A_e} \mathbf{k}(\mathbf{u})^2 d\mathrm{x}\, d\mathrm{y}, \\
\left\| \mathbf{g}(\mathbf{u}) - \mathbf{g}^{\varepsilon} \right\|^2 &\equiv \int_{A_e} \mathbf{g}(\mathbf{u})^2 d\mathrm{x}\, d\mathrm{y}
\end{aligned} \tag{9.2}$$

For such elements, the weighting coefficients are required to be small; for example, they can be set in the range of $(10^{-3} - 10^{-6}) \times (w_e, w_k, w_g)$, compared to the values used in the elements that possess strain data. These 'strainless' elements, with very small weighting coefficients, provide the requisite interpolation connectivity to the elements that have strain-sensor data. Importantly, they ensure the sufficient regularization of the *iFEM* models that have very sparse measured strain data. In a more general case, the weighting coefficients are defined per strain measure, i.e., each of the eight squared differences, between interpolated and measured strains, has its own weighting coefficient. This allows for a robust, regularized solution even when a particular measured strain component is not available or has a sufficiently unreliable value.

The remainder of the formulation follows standard finite element procedures; for brevity, this discussion is herein omitted.

NUMERICAL EXAMPLE

In this example, an aluminum rectangular plate (2 *in* × 10 *in*, 2*t* =0.1 *in*) is clamped along the left edge and is subjected to a uniform transverse shear traction $F_z = 4.5 lbf / in$ applied in the positive z direction along the right edge; the material elastic constants are $(E, \nu) = (10^7\ psi, 0.3)$.

Initially, a linear static analysis is performed using a high-fidelity mesh consisting of 1,280 S3R (three-node) shear-deformable shell elements in ABAQUS [9]. Figure 2 depicts the resulting deflection solution and the underlying FEM mesh. This reference analysis is used as a source for the simulated sensor-strain data ($\mathbf{e}_i^{\varepsilon}$, $\mathbf{k}_i^{\varepsilon}$ and $\mathbf{g}_i^{\varepsilon}$), with their values mapped onto discrete 'strain-rosette' locations within the *iFEM* meshes. The FEM displacements are used to assess the predictive capability of the *iFEM* analyses.

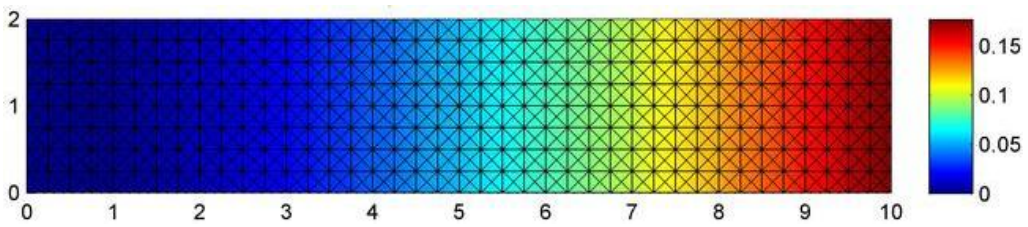

Figure 2. Deflection of a cantilevered aluminum plate subjected to a uniform transverse shear traction at the free edge ($w_{\max}^{FEM} = 0.1766\ in$).

It is noted that when the *iFEM* discretization is the same as that of the reference FEM, and if there is a one-to-one mapping of the sensor strain data from FEM onto *iFEM*, the *iFEM*-reconstructed displacement field matches the reference displacements either identically or almost identically. The practical challenge, however, is when the strain sensor data are sparse and are not available everywhere in the *iFEM* discretization domain; the models in Figures 3-5 explore such possibilities.

In Figure 3, a moderately fine mesh of *iMIN3* elements is shown where the red dots denote positions of 26 strain rosettes distributed on the top surface of the plate. Thus, only 26 elements in the discretization have sensor strains; for these elements, $(w_e, w_k, w_g) = 1$. For an element that does not have any sensor strains, its weighting coefficients are set to 10^{-5}. Figures 4 and 5 depict similar models and their predictions. In these examples, keeping the same *iMIN3* mesh, there are fewer strain rosettes used, namely 22 and 18.

(a) Strain rosettes at center of *iMIN3* elements

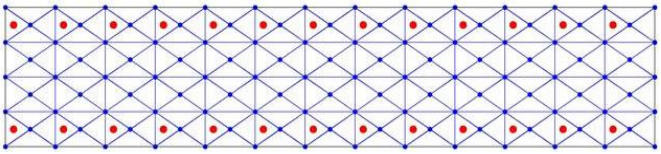

(b) w^{iMIN3} deflection

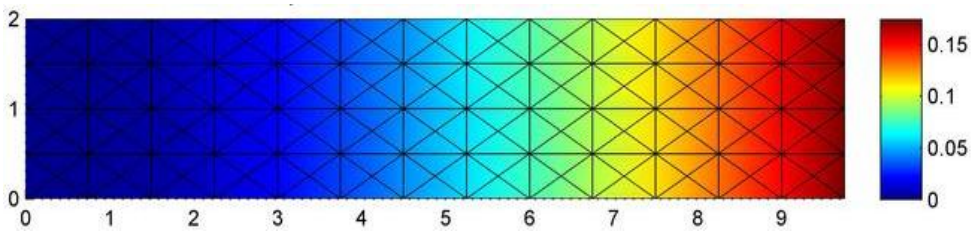

Figure 3. (a) *iMIN3* discretization using strain data from 26 strain rosettes (three strain components measured on the top surface) distributed close to plate edges; (b) *iMIN3*-reconstructed plate deflection distribution ($w_{\max}^{iMIN3} / w_{\max}^{FEM} = 0.982$).

(a) Strain rosettes at center of *iMIN3* elements

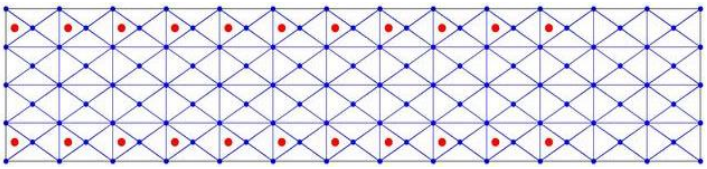

(b) w^{iMIN3} deflection

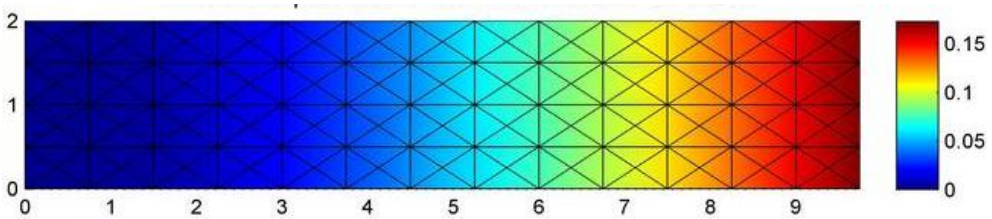

Figure 4. (a) *iMIN3* discretization using strain data from 22 strain rosettes (three strain components measured on the top surface) distributed close to plate edges; (b) *iMIN3*-reconstructed plate deflection distribution ($w_{\max}^{iMIN3} / w_{\max}^{FEM} = 0.979$).

(a) Strain rosettes at center of *iMIN3* elements

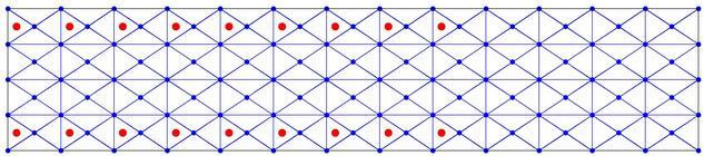

(b) w^{iMIN3} deflection

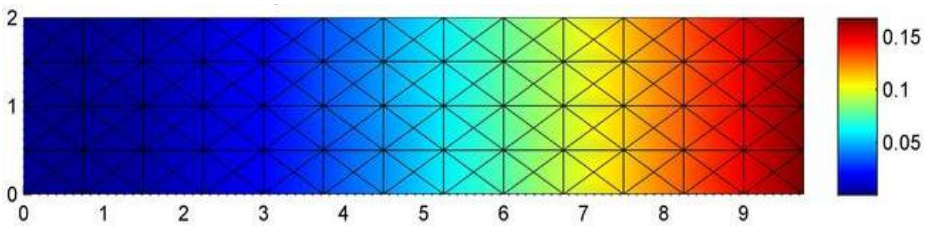

Figure 5. (a) *iMIN3* discretization using strain data from 18 strain rosettes (three strain components measured on the top surface) distributed close to plate edges; (b) *iMIN3*-reconstructed plate deflection distribution ($w_{\max}^{iMIN3} / w_{\max}^{FEM} = 0.948$).

CONCLUSIONS

A revised formulation of the inverse Finite Element Method (*iFEM*) has been presented and formulated as a user routine in the ABAQUS commercial code. The method uses arbitrarily distributed strain measurements to perform shape-sensing analyses (reconstruction of a deformed structural shape) of plate and built-up shell structures. The numerical studies included densely and sparsely distributed FBG (Fiber Bragg Grating) arrays that provide either single-core (axial) or rosette (tri-axial) strain measurements (only the rosette results have been highlighted in the paper). Various types of low- and high-fidelity discretization strategies have been explored. The numerical results have confirmed that in the absence of available strain-sensor data and under conditions of relatively sparse strain data, it is still possible to use high-fidelity discretizations to reconstruct sufficiently accurate deformed structural shapes.

REFERENCES

1. Tessler, A. and Spangler, J. L. 2003. A variational principle for reconstruction of elastic deformations in shear deformable plates and shells. NASA/TM-2003-212445.
2. Tessler, A. and Spangler, J. L. 2004. Inverse FEM for full-field reconstruction of elastic deformations in shear deformable plates and shells. SHM Conference, Munich.
3. Tessler, A. and Spangler, J. L. 2005. A least-squares variational method for full-field reconstruction of elastic deformations in shear-deformable plates and shells. *Computer Methods in Applied Mechanics and Engineering*, 194, 327-339.
4. Tessler, A. 2007. Structural analysis methods for structural health management of future aerospace vehicles. NASA/TM-2007-214871.
5. Gherlone, M. 2008. Beam inverse finite element formulation. Report LAQ-AERMEC, Politecnico di Torino.
6. Cerracchio, P., Gherlone, M., Mattone, M., Di Sciuva, M., and Tessler, A. 2010. Shape sensing of three-dimensional frame structures using the inverse finite element method. Proceedings of 5th European Workshop on SHM, Sorrento, Italy.
7. Gherlone, M., Cerracchio, P., Mattone, M., Di Sciuva, M., and Tessler, A. 2011. Dynamic shape reconstruction of three-dimensional frame structures using the inverse finite element method. Proceedings of 3rd ECCOMAS Thematic Conference on Computational Methods in Structural Dynamics and Earthquake Engineering, Corfù, Greece.
8. Tessler, A., and Hughes, T. J. R. 1985. A three-node Mindlin plate element with improved transverse shear. *Computer Methods in Applied Mechanics and Engineering*, 50: 71-101.
9. ABAQUS, Dassault Systemes Simulia Corp. (SIMULIA), Version 6.10, Providence, RI, 2010.